Clays and Clay Minerals, Vol. 47, No. 3, 375–385, 1999.

PREPARATION AND PROPERTIES OF HEMATITE WITH STRUCTURAL PHOSPHORUS

NATIVIDAD GÁLVEZ, VIDAL BARRÓN, AND JOSÉ TORRENT

Departamento de Ciencias y Recursos Agrícolas y Forestales, Universidad de Córdoba, Apdo. 3048, 14080 Córdoba, Spain

Abstract—Synthetic hematites prepared in the presence of phosphate can incorporate phosphorus (P) in forms other than phosphate adsorbed by ligand-exchange on the crystal surface. To investigate the nature of such occluded P, which is also found in some natural specimens, we prepared 13 hematites by aging ferrihydrite precipitated from $Fe(NO_3)_3$-KH_2PO_4 solutions. The P/Fe atomic ratio of the resulting hematites ranged from 0 to 3% and all incorporated significant amounts of OH. As P content is raised, particle morphology changes from rhombohedral to spindle or ellipsoid-shaped. Despite the grainy appearance in transmission electron microscope images, X-ray diffraction data indicate that the particles are single crystals. Specific surface area ranged from 66 to 91 $m^2\ g^{-1}$, partly in micropores. The intensity of the absorption bands due to Fe^{3+} ligand field transition in the visible region, as measured by the second derivative of the Kubelka-Munk function, suggests that both OH and P contribute to an Fe deficiency in the structure. Such a deficiency is also apparent from the 104/113 peak intensity ratio in the X-ray diffraction patterns. The *c* unit-cell length increases with increasing P content. The infrared spectra exhibit four bands in the P-OH stretching region (*viz.*, at 936, 971, 1005, and 1037 cm^{-1}) which suggest that occluded PO_4 possesses a low symmetry. Congruent dissolution of P and Fe was observed on acid treatment of the hematites, the dissolution rate being negatively correlated with the P content. All observations are consistent with the occluded P in the hematites being structural. A model is proposed where P occupies tetrahedral sites in the hematite structure, thus resulting in an Fe deficiency and facilitating proton incorporation.

Key Words—α-Fe_2O_3, Hematite, Color, Crystal Chemistry, Dissolution, IR Spectra, Structural P, Structure.

INTRODUCTION

The formation of Fe oxides and oxyhydroxides in aqueous environments is affected by the type and concentration of cations, anions, and neutral molecules present in solution (Cornell and Schwertmann, 1996). One such solute is (ortho)phosphate, a ubiquitous anion that interacts strongly with Fe oxides via specific adsorption (ligand exchange) with surface OH groups. Laboratory experiments showed that phosphate slows the rate of transformation of ferrihydrite to crystalline Fe oxides and influences the type of oxide product and its characteristics. Gálvez *et al.* (1999) reported that the hematite/goethite ratio in the products obtained from the transformation of ferrihydrite with coprecipitated phosphate at temperatures between 298–373 K depends on the P/Fe ratio, and the resulting hematites are spindle-shaped or ellipsoidal. These shapes are observed also in hematites formed in $FeCl_3$ systems with akaganéite as precursor if phosphate is present (Reeves and Mann, 1991; Kandori *et al.*, 1992; Morales *et al.*, 1992; Matijevic, 1993; Sugimoto *et al.*, 1993; Ocaña *et al.*, 1995; Sugimoto and Muramatsu, 1996).

Hematites prepared from Fe^{3+}-rich solutions containing phosphate incorporate significant amounts of P (Gálvez *et al.*, 1999; Serna, personal communication). Alkali treatment results in removal of only a small fraction of the phosphate in the solid phase. Since alkali treatment is considered to be effective in removing phosphate in surface complexes (Cabrera *et al.*, 1981; Torrent *et al.*, 1990), most of the phosphate appears to be in an occluded form, and the nature of this form has not been studied carefully.

In this paper we investigate the form in which P is occluded in hematites prepared from ferrihydrites with coprecipitated phosphate. In particular, we test the hypothesis that the P is structural. This investigation has geochemical relevance since many natural hematites and other Fe oxides appear to contain significant amounts of non-alkali-extractable P (Ruiz *et al.*, 1997, and unpubl. results). Thus, it is likely that the amount of P occluded in hematite reflects the P concentration in the medium in which this mineral was formed.

MATERIALS AND METHODS

Preparation of hematite with occluded P

Thirteen ferrihydrites with coprecipitated P were prepared by adding 1 M KOH (~10 $cm^3\ min^{-1}$) to 200 cm^3 of a continuosly stirred 0.135 M $Fe(NO_3)_3$ solution containing KH_2PO_4 until the pH was 4. The P/Fe atomic ratio in the solution, expressed as percentage, ranged from 0 to 3%; greater ratios were not used because they did not result in crystallization of hematite (Gálvez *et al.*, 1999). The resulting ferrihydrite suspension was centrifuged and ~190 cm^3 of the supernatant were discarded. Then, solid $Mg(NO_3)_2{\cdot}6H_2O$ and water were added to make the Mg concentration 2 M; this was done to prevent formation of goethite in the following synthesis steps (Colombo, 1993). Af-

ter readjusting pH to 4, the suspension was poured into a pyrex bottle which was placed in an oven at 373 ± 1 K. Crystallization of hematite was considered to be complete when the volume occupied by the initial gelatinous precipitate was reduced to less than one tenth of the original, and the color of the sediment was bright red. Crystallization occurred from <1 d in the P-free sample to ~5 d in the sample with P/Fe = 3%. After cooling, centrifugation, and decantation, the sediment was washed once (twice in the P-rich samples) with 0.5 M HNO_3 to dissolve any residual ferrihydrite, twice with 0.1 M KNO_3 at pH 3, and twice with 0.1 M KOH-0.5 M KNO_3 to remove phosphate adsorbed on the surface of hematite. The suspension was finally brought to the pH of maximum flocculation (7.2 to 7.4), washed four times with water, and dialyzed in deionized water. About one third of the resulting suspension was freeze-dried. The rest was stored as stock suspension and the hematite concentration was measured by evaporating 2 cm^3 at 383 K. A portion of the freeze-dried sample was heated at 1073 K for 2 h.

Physical, chemical, and mineralogical analyses

The specific surface area and the micropore surface area were determined by N_2 adsorption (BET and *t*-plot methods, respectively) with a Micromeritics ASAP 2010 surface area analyzer. Color was determined with a Varian Cary 1E spectrophotometer equipped with a diffuse reflectance attachment. To prevent particle orientation, color was measured in mixtures of 3 wt. % hematite-97 wt. % white standard $BaSO_4$. The reflectance (R) values were taken at intervals of 0.5 nm in the 380–710 nm range and converted to the CIE $L^*a^*b^*$ color parameters, as described by Barrón and Torrent (1986). The second derivative curve of the Kubelka-Munk function $[(1 - R)^2/2R]$ for this range was obtained by using a cubic spline fitting procedure applied to a series of 22 consecutive R values (Press *et al.*, 1992; Scheinost *et al.*, 1998).

To determine total Fe and P contents, the hematite was dissolved by treating 0.1 cm^3 of the stock suspension with 2 cm^3 of 11 M HCl. In the resulting solution, Fe was determined by the o-phenanthroline method (Olson and Ellis, 1982) and P by the molybdenum blue method (Murphy and Riley, 1962). The loss of water in the 293–1073 K range was examined with a Cameca thermobalance set at a heating rate of 5 K min^{-1}. The loss of water measured in this way was not significantly different from the loss measured in samples heated at 473 K for 24 h and then at 1073 for 70 h. Because of greater precision, the water loss in the 423–1073 K range measured with the thermobalance was used, together with the P/Fe ratio, to calculate the structural formula $Fe_xP_y(OH)_wO_{3-w}$, where $3x + 5y = 6 - w$.

The phosphate adsorption capacity was determined in suspensions containing 10–25 mg of hematite and 0.100 mg of P as KH_2PO_4 in 8 cm^3. After adding the phosphate and stirring the suspension for 1 min, the pH was adjusted to 6. Then, the suspension was stirred occasionally during the next 3 h, the pH readjusted to 6 and, finally, shaken in a polyethylene bottle at 3 Hz for 3 d. After centrifuging and determining the concentration of P in the supernatant, the phosphate adsorption capacity was calculated from the difference between total P added and P remaining in solution. For some dissolution experiments, hematite with the surface saturated with phosphate was prepared by adding an amount of phosphate in excess of the phosphate adsorption capacity to the hematite suspension. After 2 h, the suspension was centrifuged, the supernatant decanted, and the sediment washed with water and freeze-dried.

Transmission electron micrographs (TEM) were obtained with a Jeol JEM-200CX electron microscope after diluting small portions of the stock suspension in water and drying a drop of the resulting thin suspension on a thin film of carbon on a copper grid. Infrared (IR) spectra of KBr pellets (0.5 wt. % sample) were recorded from 380 to 4000 cm^{-1} with a Perkin-Elmer 2000 FTIR spectrometer using 4 cm^{-1} resolution and an average of 100 scans. X-ray diffraction (XRD) traces were obtained with a Siemens D5000 apparatus equipped with CoKα radiation and a graphite monochromator. The hematite samples, mixed with 10% silicon as internal standard, and prepared as self-supporting powder mounts, were scanned at appropriate angular ranges to contain the 012, 104, 110, 113, 024, 116, 018, 214, and 300 reflections at 0.02 °2θ steps and 10 s counting time. The scans were fitted to a pseudo-Voigt function (FIT program for Siemens diffractometers), from which the Cauchy and the Gauss integral breadths were derived (de Keijser *et al.*, 1983). Mean coherence length (MCL) perpendicular to a given plane (MCL_{hkl}) was calculated from the Cauchy integral breadth (corrected for the Cauchy breadth of well crystallized quartz) according to the Scherrer formula. In this formula, the values of k were taken from Stanjek (1991). The hematite a and c unit-cell lengths were derived from the positions of the nine reflections (above) and refined with a *least-squares* procedure. Oriented mineral aggregate mounts on glass slides were prepared by mixing a portion of the stock suspension containing 0.2 mg of hematite with 1 cm^3 of water, spreading the suspension on an area of ~1.5 cm^2, and letting it dry at room temperature. The diffractograms of these mounts were obtained for the appropriate angular ranges to contain the 012, 104, and 110 reflections at 0.01 °2θ steps and 15 s counting time.

Table 1. Chemical composition of the hematites.

Sample[1]	P/Fe atomic ratio × 100	Parameters of the $Fe_xP_y(OH)_wO_{3-w}$ formula			
		x	y	w	$3-w$
0.00	0.00	1.81	0.000	0.57	2.43
0.25	0.23	1.80	0.004	0.57	2.43
0.50	0.48	1.80	0.009	0.57	2.43
0.75	0.71	1.80	0.013	0.55	2.45
1.00	0.95	1.78	0.017	0.57	2.43
1.25	1.16	1.76	0.021	0.62	2.38
1.50	1.38	1.73	0.024	0.68	2.32
1.75	1.69	1.75	0.030	0.59	2.41
2.00	1.80	1.72	0.031	0.68	2.32
2.25	2.11	1.71	0.036	0.69	2.31
2.50	2.30	1.70	0.039	0.70	2.30
2.75	2.82	1.68	0.048	0.71	2.29
3.00	2.97	1.68	0.050	0.72	2.28

[1] Sample code is the atomic P/Fe ratio (in percentage) in the initial $Fe(NO_3)_3$-KH_2PO_4 solution.

Acid dissolution experiments

Two cm^3 of the stock suspension (equivalent to 10–33 mg of hematite) were added to 8 cm^3 of a magnetically stirred 8.75 M HCl-0.875 M H_2SO_4 solution at 298 K. Portions of 0.4 cm^3 were taken from the resulting suspension at times of 5 to 360 min and immediately centrifuged for 2 min at an acceleration of 1.2×10^5 m s^{-2}. Then, the concentrations of Fe and P in the supernatant were determined by the above methods.

RESULTS AND DISCUSSION

Chemical composition

Most of the Fe in the initial solutions was precipitated as ferrihydrite, which incorporated much of the P. This P was largely retained by the hematite formed from the ferrihydrite, as suggested by Table 1, which shows that the P/Fe ratio of the hematites is only slightly smaller than the P/Fe ratio of the initial solutions. These small differences in the P/Fe ratio may be due to phosphate retained by the surface of the hematite resulting from the crystallization ferrihydrite. Such phosphate was removed when, in the course of the preparation of the stock suspension, the hematite was washed with 0.1 M KOH. Hereafter, the term "occluded P" will be used to refer to the non-hydroxyl-extractable P that is incorporated in the hematite.

All the hematites incorporate hydroxyl, as indicated by the significant value of w in the hypothetical structural formula $Fe_xP_y(OH)_wO_{3-w}$ (Table 1). The OH content is positively and significantly correlated with the P content ($r^2 = 0.78$).

Morphological and surface properties

The TEM images show a gradual change in particle morphology as P content increases (Figure 1; Table 2), from nearly equidimensional (apparently cube-like) crystals of 60–70 nm for P/Fe = 0 to spindles or ellipsoids with a length of 170–230 nm and a maximum width of 40–60 nm for P/Fe >2.5%. The face index of the surface planes of the cube-like hematites is (012), as suggested by the high oriented mount/powder intensity ratio for the 012 reflection (Figure 2). This suggests that these particles are imperfect rhombohedra with {012} faces, similar to some synthetic hematites (Sugimoto *et al.*, 1993). The long axis of the spindle-shaped hematites corresponds to the [001] direction because the value of such ratio is large for the 110 reflection and small for the 104 reflection (which corresponds to a plane at a high angle to 110) (Figure 2). A similar orientation was observed by Reeves and Mann (1991).

All hematites exhibit a "grainy" appearance, with the apparent grains of about one tenth of the particle size. These grains are elongated in the [001] direction for spindle-shaped particles. The mean coherence lengths (MCLs) perpendicular to the (012), (104), and (110) planes (Table 2) are generally similar to the dimensions of the particles as observed in TEM images, suggesting that the apparent grains diffract coherently. Therefore, the particles are essentially monocrystalline, as is common with hematites prepared in the presence of phosphate by the sol-gel method (Sugimoto *et al.*, 1998). The separation between the grains suggested by the TEM images may be limited to the grains on the particle surface.

The specific surface area (Table 2) ranges from 66 to 91 m^2 g^{-1} and bears little relation with P/Fe for the samples with P/Fe <2.5%. For the two samples with P/Fe >2.75%, the values are smaller (45 and 58 m^2 g^{-1}). In the latter samples, the proportion of the total surface area in micropores is <30%, which contrasts with the greater proportion (>45%) observed in other samples. The contribution of microporosity and surface rugosity to the surface area (as also suggested by the TEM images) is substantial, given that the specific surface area calculated on the basis of the external particle shape ranges from 15 to 20 m^2 g^{-1}. The phosphate adsorption capacity on a surface area basis (Table 2) ranges from 1.5 to 2.5 μmol P m^{-2} and shows little relationship with P/Fe. These values are consistent with the TEM images, which suggest the presence of a significant proportion of the most active P-adsorbing faces, such as the (012) and the (110) (Colombo *et al.*, 1994; Barrón and Torrent, 1996).

Upon heating at 1073 K, the granular appearance of the particles was lost, the surface became smooth, and vesicles, probably caused by the escape of water, appeared (Figure 3). The specific surface area of the heated samples (not shown) ranged from 15 to 20 m^2 g^{-1}, consistent with the observed sizes based on TEM data and with the absence of surface rugosity and micropores.

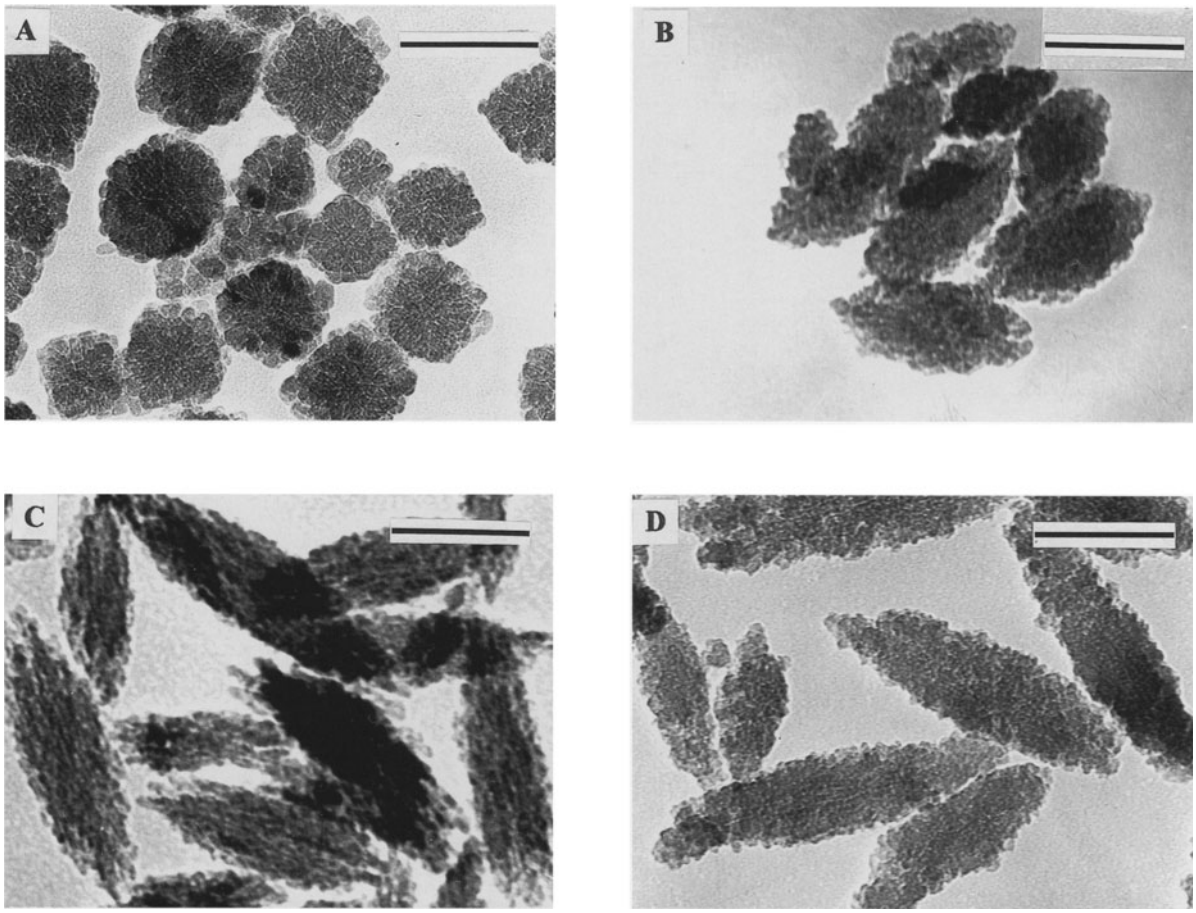

Figure 1. TEM images of hematite samples (A) 0.00, (B) 1.00, (C) 2.00, and (D) 3.00. Bar represents 100 nm.

Table 2. Morphological and surface properties of hematite.

Sample	Size and shape (TEM)	Mean coherence lengths ⊥ to the given planes: Original samples (012)	(104)	(110)	Samples heated at 1073 K (012)	(104)	(110)	Specific surface area	Micro-pore surface area	Phosphate adsorption capacity
		nm						$m^2\ g^{-1}$		µmol m^{-2}
0.00	60–70 nm cube-like	88	81	73	133	123	101	70	38	2.2
0.25		116	104	82	94	85	78	87	52	1.8
0.50	120 × 70 nm spindles	119	107	85	111	74	59	77	43	2.0
0.75		108	105	74	149	70	58	81	45	1.9
1.00	120 × 65 nm spindles	115	107	74	127	57	46	71	34	1.8
1.25		106	97	72	86	68	52	84	42	1.7
1.50	180 × 70 nm spindles	91	91	66	134	102	70	91	44	1.8
1.75		107	104	71	98	102	65	66	31	1.7
2.00	150 × 65 nm spindles	100	95	68	97	92	64	90	40	1.7
2.25		82	88	61	100	105	59	89	39	1.7
2.50	200 × 50 nm spindles	90	86	59	87	84	57	90	40	1.5
2.75		90	93	67	153	89	60	58	18	1.5
3.00	200 × 55 nm spindles[1]	84	82	62	86	83	59	45	11	2.5

[1] Partly ellipsoids.

https://doi.org/10.1346/CCMN.1999.0470314 Published online by Cambridge University Press

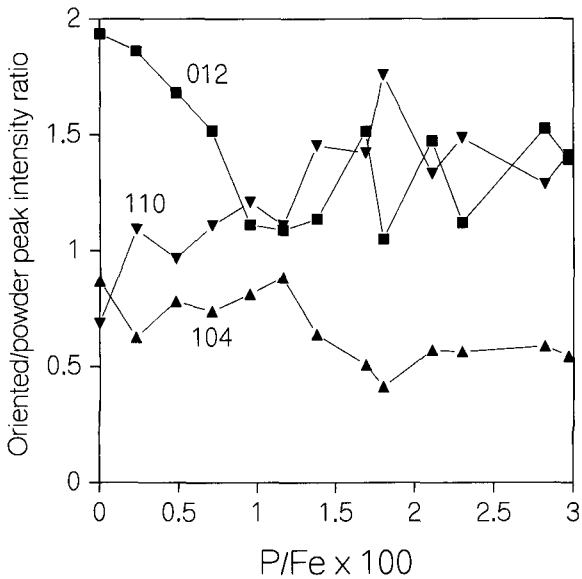

Figure 2. The ratio between the intensities of the XRD peaks of the oriented mineral aggregates and those of the corresponding powder samples as a function of P/Fe for the 012, 110, and 104 reflections.

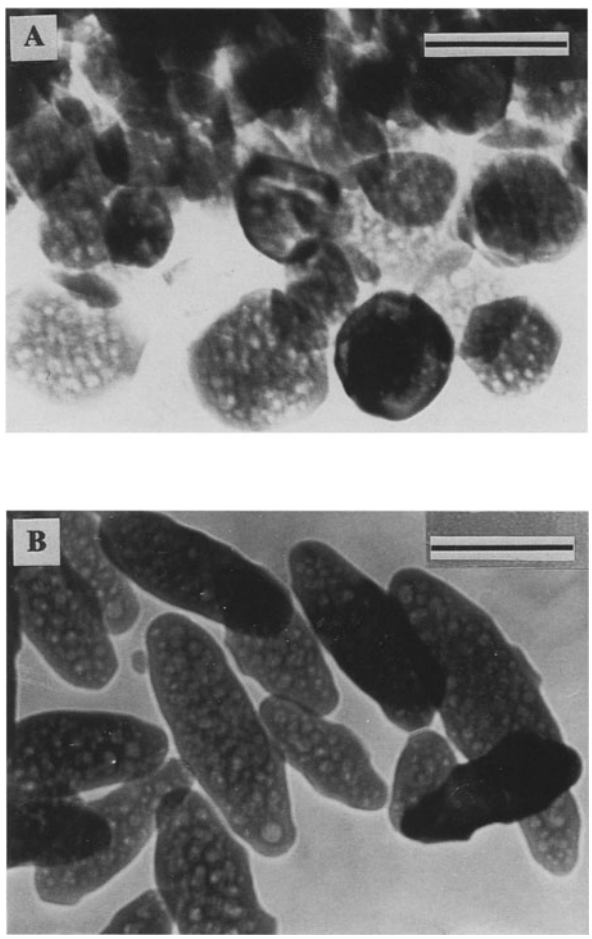

Figure 3. TEM images of two hematites heated at 1073 K: (A) 1.00, and (B) 2.00. Bar represents 100 nm.

Color

The color of the hematites was bright red, which is characteristic of hematites in the 50–200 nm size range (Torrent and Schwertmann, 1987). Upon heating to 1073 K, there was a change (Figure 4) to less saturated, more purple hues (lower a^* and b^* values). This effect increased markedly with decreasing P/Fe, and thus the pure hematite showed a dark purple color and the hematites with P/Fe >2.5% were bright red. Purple hues in hematite are associated with large particle sizes (Morris *et al.*, 1985). So, it can be hypothesized that particles sintered at 1073 K, the degree of sintering decreased with increasing P content. It is possible that P makes hematite more refractory or, by means of its influence on the initial particle shape, makes the particle contacts less favorable to sintering. In fact, when sintering was prevented by thoroughly mixing a portion of the hematite suspension with $BaSO_4$ before heating at 1073 K (to decrease the number of hematite-hematite contacts), color changed little regardless of P/Fe (results not shown).

Minima of the second derivative curves of the $(1 - R)^2/2R$ function, which indicate the position of the absorption bands due to Fe^{3+} ligand field transitions, are observed at ~405, 425–435, 445, 488, and 538 nm (Figure 5). The bands at 405, 445, and 538 nm can be assigned to hematite and correspond respectively to the $^6A_1 \rightarrow {}^4T_2$ (^4D), $^6A_1 \rightarrow {}^4E{}^4A_1$ (^4G), and $2(^6A_1) \rightarrow 2(^4T_1)$ electron transitions (Sherman and Waite, 1985). The 425–435 and 488 nm bands have a smaller intensity than the former ones and are typical of the goethite $^6A_1 \rightarrow {}^4E{}^4A_1$ (^4G) and $2(^6A_1) \rightarrow 2(^4T_1(^4G))$ transitions. Therefore, the hematites behave optically as if they contain a goethite impurity. Because no goethite was detected by XRD in any of the samples, this "optical goethitic component" is probably due to structural and surface hydroxyls.

The position of the absorption bands is not related to the P/Fe ratio. To measure band intensity, we took the band amplitude, defined as the difference in ordinate between the corresponding minimum and the next maximum at longer wavelength (*e.g.*, the difference in ordinate between the hematite minimum at 538 nm and the next maximum at 574 nm). The relative band intensity changes with the P/Fe ratio. In particular, the $2(^6A_1) \rightarrow 2(^4T_1)$ (538 nm) hematite band, which is assigned to Fe^{3+}-Fe^{3+} pair excitations, decreases with P/Fe, which indicates decreasing degree of Fe^{3+}-Fe^{3+} coupling. The magnitude of the optical goethitic component relative to hematite can be quantified as the 488–504 nm (goethite) to the 538–574 nm (hematite) band amplitude ratio. This ratio increases with increasing P/Fe in the unheated hematites (Figure 6). Since OH content increases with increasing P/Fe, this result

https://doi.org/10.1346/CCMN.1999.0470314 Published online by Cambridge University Press

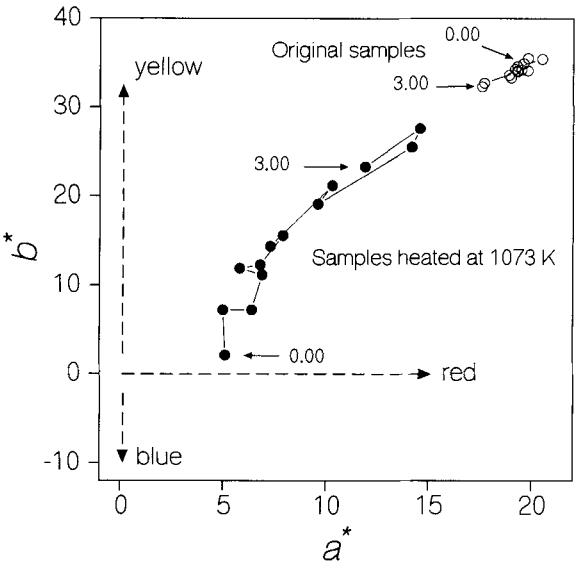

Figure 4. The CIE a^* and b^* parameters of mixtures of hematite (3 wt. %) and white standard, $BaSO_4$ (97 wt. %), for the untreated samples and after heating at 1073 K.

is consistent with the hypothesis that OH creates the aforementioned optical goethitic component.

The position of the absorption bands changed little when the samples were heated at 1073 K. As with the unheated samples, the (488–504 nm)/(538–574 nm) band amplitude ratio increases significantly with increasing P/Fe (Figure 6). This increase cannot be due to differences in structural OH, which is eliminated by heating, nor to differences in surface adsorbed hydroxyl, because the samples have similar surface area. Therefore, in analogy with OH, the P occluded in the hematite particles produces an optical goethitic effect. We did not observe any significant change in the band amplitude ratio when hematite was surface-saturated with phosphate, *i.e.*, adsorbed phosphate does not affect the second derivative spectrum. The slope of the regression line of the amplitude ratio against P/Fe is steeper relative to that of the heated samples, consistent with both OH and occluded P contributing to the optical goethitic effect.

Structural properties

The *c* unit-cell length is significantly and positively correlated with P/Fe (Table 3; Figure 7); this effect was noted also by Ocaña *et al.* (1995). In contrast, the *a* length varies little (Table 3) and is unrelated to P/Fe. The value of *c* in the hematites heated at 1073 K is also correlated with P/Fe, but the regression line has a lower slope (Figure 7). This difference in slope can be explained by the effect structural hydroxyl has in increasing *c* (Stanjek and Schwertmann, 1992). However, given the high covariance between P/Fe and hydroxyl content, the relative contribution of P and hy-

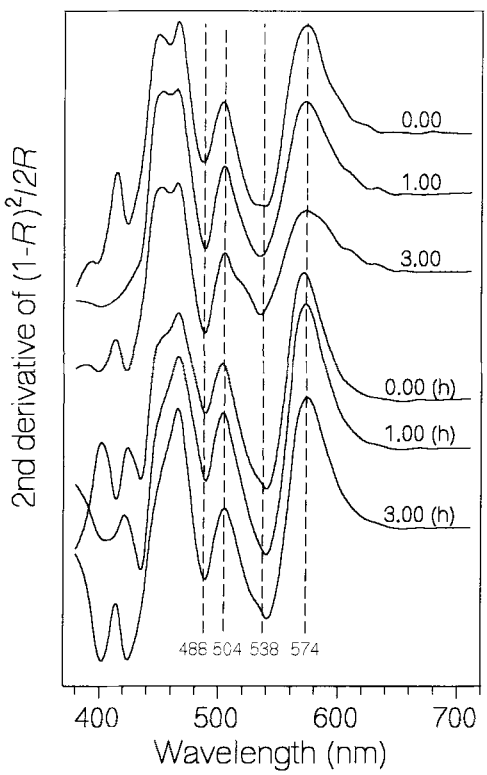

Figure 5. Second-derivative curves of the Kubelka-Munk function of hematite-$BaSO_4$ (3–97 wt. %) mixtures for hematite samples 0.00, 1.00, and 3.00. The curves for the mixtures heated at 1073 K are indicated by 1.00 (h), 2.00 (h), and 3.00 (h).

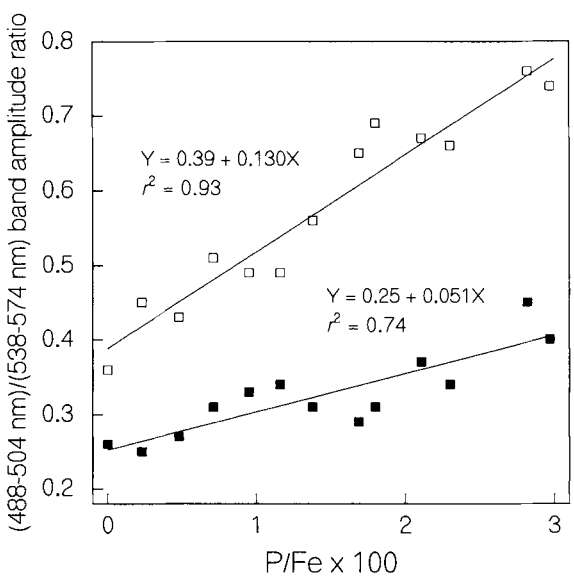

Figure 6. The (488–504 nm)/(538–574 nm) band amplitude ratio in the second derivative spectra of the Kubelka-Munk function of hematite-$BaSO_4$ mixtures as a function of P/Fe. Open symbols: untreated hematite; solid symbols: hematite heated at 1073 K.

https://doi.org/10.1346/CCMN.1999.0470314 Published online by Cambridge University Press

Table 3. Unit cell parameters of hematite.

Sample	Original samples		Samples heated at 1073 K	
	a (nm)	*c* (nm)	*a* (nm)	*c* (nm)
0.00	0.5032	1.3776	0.5034	1.3744
0.25	0.5031	1.3785	0.5033	1.3746
0.50	0.5035	1.3793	0.5037	1.3748
0.75	0.5031	1.3788	0.5036	1.3755
1.00	0.5033	1.3801	0.5035	1.3756
1.25	0.5032	1.3800	0.5034	1.3754
1.50	0.5028	1.3800	0.5035	1.3758
1.75	0.5031	1.3805	0.5034	1.3759
2.00	0.5031	1.3809	0.5034	1.3759
2.25	0.5033	1.3814	0.5034	1.3764
2.50	0.5032	1.3811	0.5033	1.3762
2.75	0.5029	1.3828	0.5030	1.3762
3.00	0.5028	1.3824	0.5031	1.3767

droxyl to the increase in *c* cannot be determined from the regression analysis.

Wolska (1981) and Stanjek and Schwertmann (1992) showed that structural OH in hematite (and the resulting Fe deficiency in the cationic substructure) can be detected by a reduction of the ratio between the intensities of the *hkl* and the 113 X-ray reflections (I_{hkl}/I_{113}), since the 113 reflection is independent of the cations. In our case, I_{hkl}/I_{113} is negatively correlated with P/Fe, as seen for the 104 reflection (Figure 8). This is consistent with the positive correlation between OH content and P/Fe. Interestingly, the negative correlation persists after dehydroxylating the samples at 1073 K (Figure 8), suggesting that P also produces structural Fe deficiency.

Figure 8 shows the I_{104}/I_{113} ratio calculated by Rietveld simulation of the X-ray pattern (RIETAN; Izumi, 1993) as a function of P/Fe for: (1) hematites containing P in tetrahedral sites (but no OH), and (2) hematites without P but with structural OH in amounts equivalent to those of the unheated samples. The sum of the slope of these two lines is similar to the slope of the line for the unheated hematites. This further supports the hypothesis that both OH and P contribute to structural Fe deficiency.

Selected IR spectra of the hematites are shown in Figure 9. The spectra hematites containing P show four distinctive and relatively narrow bands in the P–O(H) stretching region, at ~936, 971, 1005, and 1037 cm^{-1}. The intensities of these bands relative to those of the hematite bands increase with increasing P content. Saturation of the surface of the hematites with phosphate produces relatively broad bands at 1015 and 1105 cm^{-1} (but not at the former frequencies), as illustrated in Figure 9 by the P-free sample; these two bands are close to those reported for diffuse reflectance IR spectra of phosphated hematites (Persson *et al.*, 1996). These observations are interpreted as evidence for the low symmetry of the occluded PO_4 units relative to PO_4 ions adsorbed on the surface. Alternatively, occluded P may exhibit higher symmetry but be present in more than one environment.

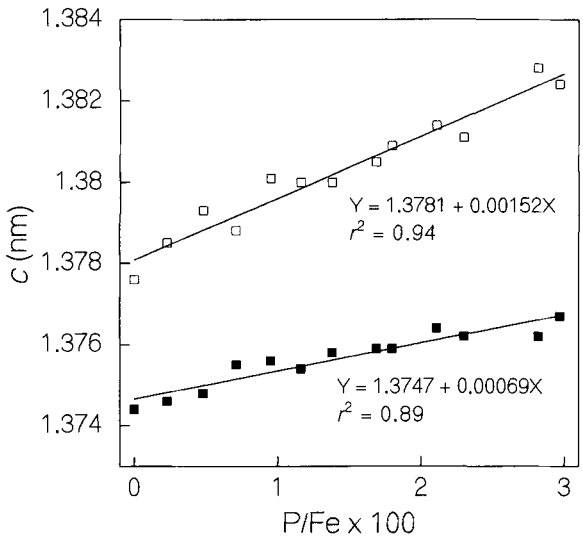

Figure 7. The *c*-cell length as a function of P/Fe. Open symbols: untreated hematite; solid symbols: hematite heated at 1073 K.

The hematites heated at 1073 K show four bands at 926 cm^{-1} (weak), 960 cm^{-1} (very weak), 1000 cm^{-1} (very weak), and 1032 cm^{-1}. These bands are slightly displaced to lower frequencies relative to the bands of the unheated hematites and are weaker than the latter.

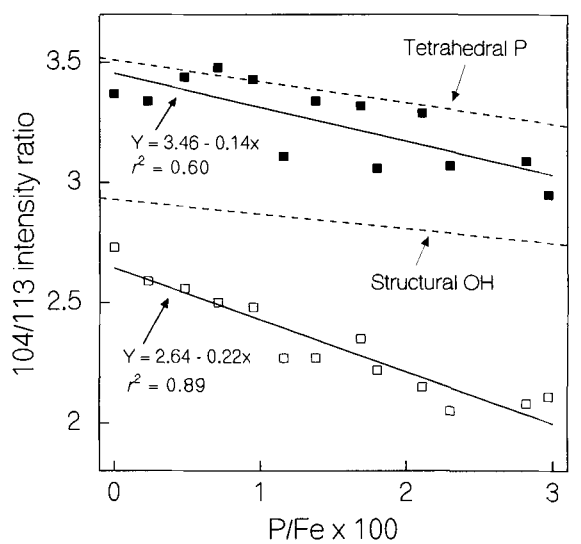

Figure 8. The ratio of the 104 to the 113 reflection from XRD data as a function of P/Fe. Open symbols: untreated hematite; solid symbols: hematite heated at 1073 K. The figure also shows the ratios obtained from Rietveld calculations based on hematite without OH and with P in tetrahedral position (upper dash line) and for hematite without P but with OH in amounts equal to that of the studied samples (lower dash line).

https://doi.org/10.1346/CCMN.1999.0470314 Published online by Cambridge University Press

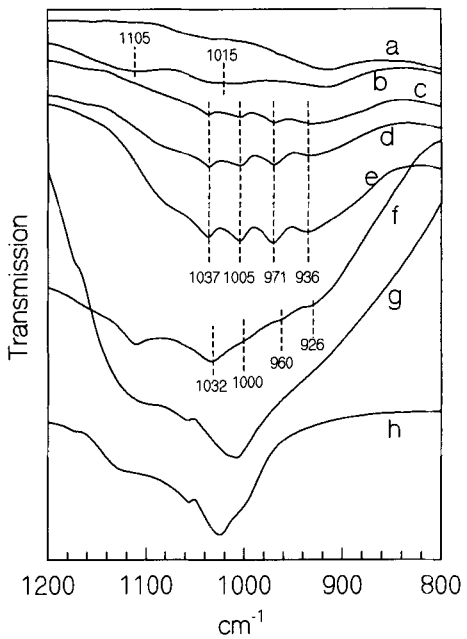

Figure 9. Infrared spectra of samples (a) 0.00, (b) phosphated 0.00, (c) 1.00, (d) 2.00, (e) 3.00, (f) 3.00 heated at 1073 K, (g) phosphated ferrihydrite heated at 1073 K, and (h) strengite heated at 1073 K.

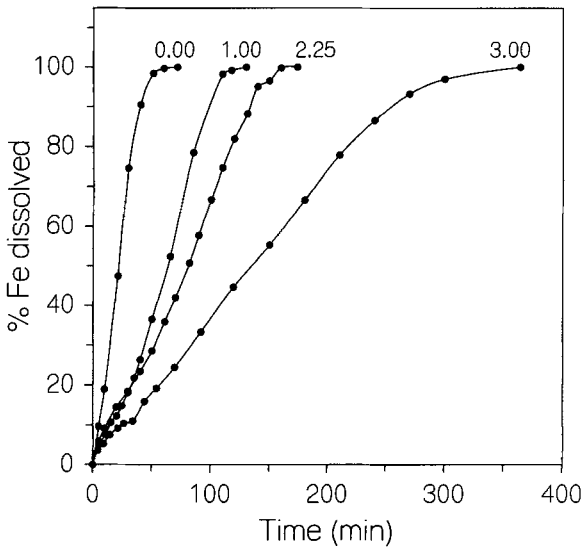

Figure 10. Acid dissolution curves of hematite samples 0.00, 1.00, 2.25, and 3.00.

This decrease in intensity in the P–(OH) stretching region is likely associated with an increase of symmetry caused by loss of OH. The spectra of the heated hematites differ clearly from the spectra of two products that contain a crystalline $FePO_4$ phase and are dehydroxylated, *viz.*, P-saturated ferrihydrite and strengite ($FePO_4 \cdot 2H_2O$) heated at 1073 K (Figure 9).

Acid dissolution

The dissolution curves are generally sigmoidal (Figure 10), *i.e.*, they indicate an acceleration of dissolution followed by deceleration of dissolution. This shape is characteristic of many hematite studies (Cornell and Giovanoli, 1993) and is explained by the increase in surface area as the result of enlargement of pores in the hematite after initial dissolution (Weidler *et al.*, 1998). The presence of P increased markedly the time needed for dissolution (Figure 10). To compare samples, we used the initial dissolution rate, which was computed as the slope of the regression line fitted to 3–5 aligned points in the range 2–20% total Fe dissolved. This rate (calculated on a surface area basis) decreases with increasing P/Fe (Figure 11).

The plot of P dissolved against Fe dissolved is always close to the 1:1 line, as illustrated in Figure 12. This plot indicates either true congruent dissolution or P dissolves preferentially to Fe during the initial period, but the phosphate that is released is mostly readsorbed on the surface of the hematite. To dismiss the possibility that phosphate is readsorbed, we saturated the P-free hematite with phosphate and dissolved it in acid. The corresponding dissolution curve was markedly convex towards the *y*-axis (Figure 12). Therefore, the surface phosphate desorbed in the initial hematite dissolution stages remained largely in solution. This lack of readsorption may be due to the strong competition between phosphate and sulfate (which is present in the acid mixture used in the experiments) for the adsorption sites on the hematite surface. Consequently, dissolution is congruent.

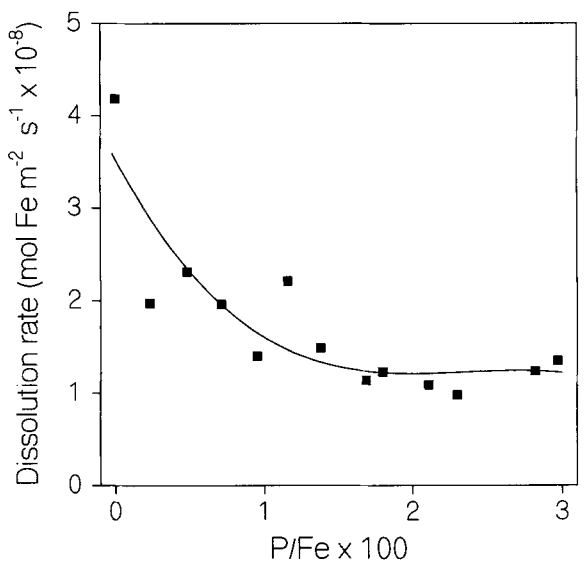

Figure 11. Initial hematite dissolution rate as a function of P/Fe.

https://doi.org/10.1346/CCMN.1999.0470314 Published online by Cambridge University Press

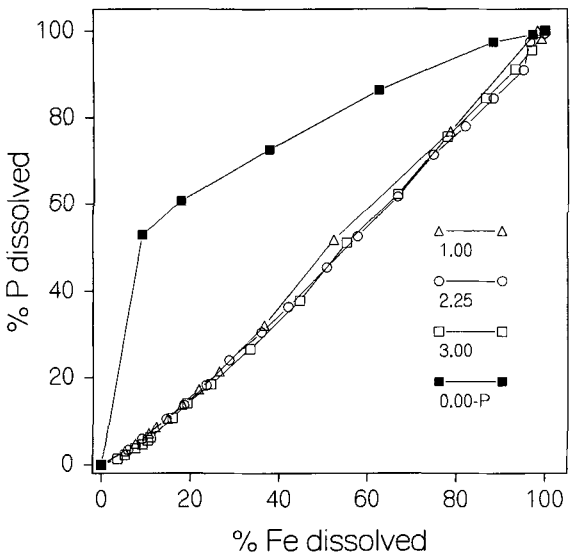

Figure 12. Percent P dissolved against percent Fe dissolved in HCl-H_2SO_4 for samples 0.00, 1.00, 2.25, 3.00, and phosphated 0.00.

DISCUSSION

Congruent dissolution of P and Fe indicates that the occluded P is evenly distributed in the hematite crystals. One possibility is that P occurs in the form of clusters of phosphate ions adsorbed on walls of micropores. These micropores are not accessible from the outer solution and are evenly distributed within the particle. However, TEM images and XRD data appear to indicate that micropores separating subcrystals are confined to the surface of the particles, and one would expect the PO_4 ions adsorbed on them to be released in the first dissolution stages, which is not the case.

The IR data suggest (see above) that the occluded PO_4 units have a lower symmetry relative to that of the adsorbed PO_4 units. The latter usually possess high symmetry (*e.g.*, C_{3v}), as suggested by Persson *et al.* (1996) for protonated monodentate complexes on goethite surfaces. Therefore, to be consistent with the IR data, if the occluded PO_4 units are adsorbed on micropore walls, they will have a molecular configuration much different from that of the PO_4 adsorbed on the external crystal surface. This, however, is an *ad-hoc* explanation not supported by other data.

Another hypothesis consistent with P-Fe congruent dissolution is the presence of a $FePO_4$ nanophase (*e.g.*, strengite) evenly distributed in the hematite particles. However, how such a phase could be intimately mixed with a hematite monocrystal is difficult to visualize.

Neither of the above hypotheses accounts for the change that P causes in the *c* unit-cell length, since the structure of a hematite crystallite is unlikely to be influenced by adsorbed phosphate or an adjacent $FePO_4$ nanophase. Moreover, these forms of PO_4 are unlikely to cause the Fe deficiency indicated by the I_{hkl}/I_{113} ratio (Figure 8).

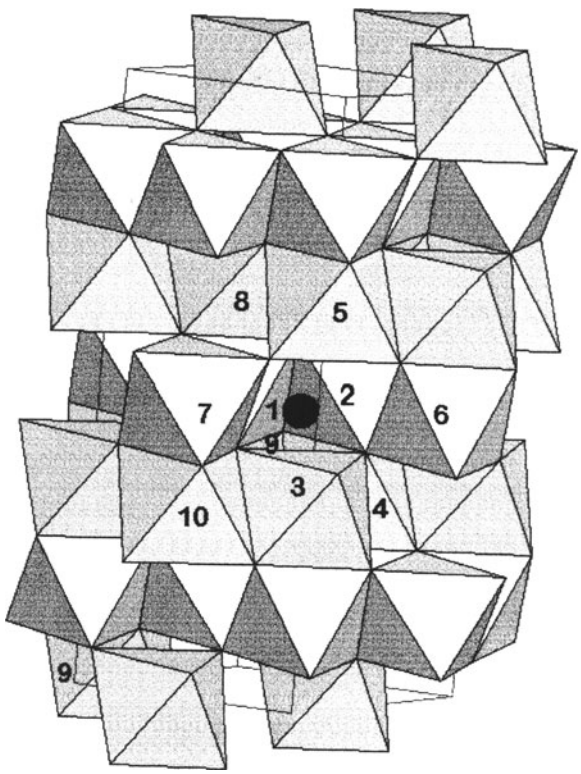

Figure 13. Model of a unit cell of hematite with P in one tetrahedral site. The distances of the P atom (black circle) to the Fe atoms of the neighboring octahedra are shown. P-Fe distances for the labelled octahedra are as follows: octahedron 1, 0.16 nm; 2, 0.19 nm; 3, 0.22 nm; 4, 0.26 nm; 5, 0.31 nm; 6, 0.34 nm; 7, 0.35 nm; 8, 0.36 nm; 9, 0.36 nm; 10, 0.39 nm.

The most simple and reasonable hypothesis is that the occluded P is mostly structural. This hypothesis is consistent not only with the relationship between the *c* dimension and P/Fe, but also with the low degree of molecular symmetry of the occluded PO_4, a fact commonly observed for PO_4 confined in crystal lattices (Persson *et al.*, 1996). If P is in the hematite structure, the regressions of *y* on *x* and *w* in the hypothetical structural formulae of Table 1 indicate that, per each additional P atom incorporated in the hematite, ~2.9 atoms of Fe are lost and 3.6 oxygens are replaced by hydroxyls. The existence of a Fe deficiency due to structural P, already suggested by the decrease in the I_{hkl}/I_{113} ratio, is further substantiated by the increase in the ratio between the amplitudes of the goethitic $2(^6A_1) \rightarrow 2(^4T_1(^4G))$ (488 nm) and the hematite $2(^6A_1) \rightarrow 2(^4T_1)$ (538 nm) bands. These bands are assigned to a double exciton process, which is more intense in hematite than in goethite because the strength of the magnetic coupling between face-sharing FeO_6 octahedra in hematite is greater than that of the edge-sharing FeO_6 octahedra in goethite. Thus, Fe deficiency

https://doi.org/10.1346/CCMN.1999.0470314 Published online by Cambridge University Press

has a greater effect on the hematite band than on the band assigned to the optical goethitic component because each FeO_6 octahedron in hematite shares one face with a (first) neighbor. Finally, the decrease of the Fe dissolution rate with increasing P content is consistent with Fe deficiency and the structural changes that P may create, but it is unlikely if the samples consist of a similar pure hematite admixed with a $FePO_4$ nanophase.

A simple structural model accounting for the above observations is shown in Figure 13. The P atoms occupy the tetrahedral sites of the hematite. The O, (OH) ions at the corners of the tetrahedron are shared with a total of ten octahedra (numbered 1 to 10 in Figure 13). Occupancy of the tetrahedral site by P results probably in the loss of some or all of the three closest Fe ions, which correspond to octahedra 1, 2, and 3 in the case of a structure not distorted by the incorporation of P. The resulting charge deficit is compensated by additional protons associated with the oxygen ions of the closest octahedra.

ACKNOWLEDGMENTS

This research was supported by the Spanish C.I.C.Y.T., Project AMB94-0322. The senior author acknowledges the award of a research grant by the Spanish Plan Nacional I+D. U. Schwertmann, Technische Universität München, and S. Myneni, Lawrence Berkeley National Laboratory, Berkeley, made useful comments on an earlier version of this paper. The authors are indebted to H. Stanjek, Technische Universität München, for his suggestions and calculations with the RIETAN program.

REFERENCES

Barrón, V. and Torrent, J. (1986) Use of the Kubelka-Munk theory to study the influence of iron oxides on soil colour. *Journal of Soil Science*, **37,** 499–510.

Barrón, V. and Torrent, J. (1996) Surface hydroxyl configuration of various crystal faces of hematite and goethite. *Journal of Colloid and Interface Science*, **177,** 407–410.

Cabrera, F., de Arambarri, P., Madrid, L., and Toca, C.G. (1981) Desorption of phosphate from iron oxides in relation to equilibrium pH and porosity. *Geoderma*, **26,** 203–216.

Colombo, C. (1993) Adsorción y desorción del fosfato en hematites de diferentes propiedades morfológicas y cristalinas. Ph.D. thesis, Univ. Córdoba, Córdoba, Spain, 118 pp.

Colombo, C., Barrón, V., and Torrent, J. (1994) Phosphate adsorption and desorption in relation to morphology and crystal properties of synthetic hematites. *Geochimica et Cosmochimica Acta*, **58,** 1261–1269.

Cornell, R.M. and Giovanoli, R. (1993) Acid dissolution of hematites of different morphologies. *Clay Minerals*, **28,** 223–232.

Cornell, R.M. and Schwertmann, U. (1996) *The Iron Oxides*. VCH, Weinheim, 573 pp.

de Keijser, T.H., Mittemeijer, E.J., and Rozendaal, H.C.F. (1983) The determination of crystallite size and lattice-strain parameters in conjunction with the profile-refinement method for the determination of crystal structures. *Journal of Applied Crystallography*, **16,** 309–316.

Gálvez, N., Barrón, V., and Torrent J. (1999) Effect of phosphate on the crystallization of hematite, goethite, and lepidocrocite from ferrihydrite. *Clays and Clay Minerals*, **47,** 304–311.

Izumi, F. (1993) Rietveld analysis programs RIETAN and PREMOS and special applications. In *The Rietveld Method*, R.A. Young, ed., Oxford University Press, Oxford, 236–253.

Kandori, K., Uchida, S., and Kataoka, S. (1992) Effects of silicate and phosphate ions on the formation of ferric oxide hydroxide particles. *Journal of Materials Science*, **27,** 719–728.

Matijevic, E. (1993) Preparation and properties of uniform size colloids. *Chemistry of Materials*, **5,** 412–426.

Morales, M.P., González-Carreño, T., and Serna, C.J. (1992) The formation of α-Fe_2O_3 monodispersed particles in solution. *Journal of Materials Research*, **7,** 2538–2545.

Morris, R.V., Lauer, H.V., Lawson, C.A., Gibson, E.K., Nace, G.A., and Stewart, C. (1985) Spectral and other physicochemical properties of submicron powders of hematite (α-Fe_2O_3), maghemite (γ-Fe_2O_3), magnetite (Fe_3O_4), goethite (α-FeOOH), and lepidocrocite (γ-FeOOH). *Journal of Geophysical Research*, **90,** 3126–3144.

Murphy, J. and Riley, J.P. (1962) A modified single solution method for the determination of phosphate in natural waters. *Analytica Chimica Acta*, **27,** 31–36.

Ocaña, M., Morales, M.P., and Serna, C.J. (1995) The growth mechanism of α-Fe_2O_3 ellipsoidal particles in solution. *Journal of Colloid and Interface Science*, **171,** 85–91.

Olson, R.V. and Ellis, R., Jr. (1982) Iron. In *Methods of Soil Analysis. Part 2, 2nd edition*, A.L. Page, R.H. Miller, and D.R. Keeney, eds., American Society of Agronomy and Soil Science Society of America, Madison, Wisconsin, 301–312.

Persson, P., Nilsson, N., and Sjöberg, S. (1996) Structure and bonding of orthophosphate ions at the iron oxide-aqueous interface. *Journal of Colloid and Interface Science*, **177,** 263–275.

Press, W.H., Teukolsky, S.A., Vetterling, W.T., and Flannery, B.P. (1992) *Numerical Recipes in Fortran*. Cambridge University Press, Cambridge, 963 pp.

Reeves, N.J. and Mann, S. (1991) Influence of inorganic and organic additives on the tailored synthesis of iron oxides. *Journal of the Chemical Society, Faraday Transactions*, **87,** 3875–3880.

Ruiz, J.M., Delgado, A., and Torrent, J. (1997) Iron-related phosphorus in overfertilized European soils. *Journal of Environmental Quality*, **26,** 1548–1554.

Scheinost, A.C., Chavernas, A., Barrón, V., and Torrent, J. (1998) Use and limitations of second-derivative diffuse reflectance spectroscopy in the visible to near-infrared range to identify and quantify Fe oxides in soils. *Clays and Clay Minerals*, **46,** 528–537.

Sherman, D.M. and Waite, T.D. (1985) Electronic spectra of Fe^{3+} oxides and oxide hydroxides in the near IR to near UV. *American Mineralogist*, **70,** 1262–1269.

Stanjek, H. (1991) Aluminium- und Hydroxylsubstitution in synthetischen und natürlichen Hämatiten. Ph.D. thesis, Tech. Univ. München, München, Germany, 194 pp.

Stanjek, H. and Schwertmann, U. (1992) The influence of aluminum on iron oxides. Part XVI: Hydroxyl and aluminum substitution in synthetic hematites. *Clays and Clay Minerals*, **40,** 347–354.

Sugimoto, T. and Muramatsu, A. (1996) Formation mechanism of monodispersed Fe_2O_3 particles in dilute $FeCl_3$ solutions. *Journal of Colloid and Interface Science*, **184,** 626–638.

Sugimoto, T. Muramatsu, A., Sakata, K., and Shindo, D. (1993) Characterization of hematite particles of different

shapes. *Journal of Colloid and Interface Science*, **158,** 420–428.

Sugimoto, T., Wang, Y., Itoh, H., and Muramatsu, A. (1998) Systematic control of size, shape and internal structure of monodisperse α-Fe_2O_3 particles. *Colloids and Surfaces*, **134,** 265–279.

Torrent, J. and Schwertmann, U. (1987) Influence of hematite on the color of red beds. *Journal of Sedimentary Petrology*, **57,** 682–686.

Torrent, J., Barrón, V., and Schwertmann, U. (1990) Phosphate adsorption and desorption by goethites differing in crystal morphology. *Soil Science Society of America Journal*, **54,** 1007–1012.

Weidler, P.G., Degovics, G., and Laggner, P. (1998) Surface roughness created by acidic dissolution of synthetic goethite monitored with SAXS and N_2-adsorption isotherms. *Journal of Colloid and Interface Science*, **197,** 1–8.

Wolska, E. (1981) The structure of hydrohematite. *Zeitschrift für Kristallographie*, **154,** 69–75.

(Received 22 September 1998; accepted 1 February 1999; Ms. 98-117)